RSC Advances

PAPER

View Article Online
View Journal | View Issue

Cite this: *RSC Adv.*, 2021, **11**, 20070

Mechanistic insights into the insertion and addition reactions of group 13 analogues of the six-membered N-heterocyclic carbenes: interplay of electrophilicity, basicity, and aromaticity governing the reactivity†

Zheng-Feng Zhang[a] and Ming-Der Su *[ab]

Three fundamental concepts (aromaticity/basicity/electrophilicity), being heavily used in modern chemistry, have been applied in this work to study the chemical reactivity of six-membered-ring group 13 N-heterocyclic carbenes (**G13-6-Rea**; G13 = group 13 elements) using density functional theory (BP86-D3(BJ)/def2-TZVP). **G13-6-Rea** is isolobal to benzene. Two model reactions have been used in the present study: the insertion reaction of **G13-6-Rea** with methane and the [1 + 2] cycloaddition reaction of **G13-6-Rea** with ethene. Our theoretical analysis reveals that the chemical reactivity of **B-6-Rea**, **Al-6-Rea**, and **Ga-6-Rea** is governed by their HOMO (the sp^2-σ lone pair orbital on the G13 element), and thus they can be considered nucleophiles. Conversely, the chemical behavior of **In-6-Rea** and **Tl-6-Rea** is determined by their LUMO (the vacant p-π orbital on the G13 element), and thus they can be considered electrophiles. On the basis of the VBSCD (valence bond state correlation diagram) model and ASM (activation strain model), this theoretical evidence demonstrates that the origin of activation barriers for the above model reactions is due to the atomic radius of the pivotal group 13 element in the six-membered-ring of **G13-6-Rea**. Accordingly, our theoretical conclusions suggest that the lower the atomic number and the smaller the atomic radius of the G13 atom, the higher the aromaticity of the six-membered-ring of **G13-6-Rea** and the smaller the singlet–triplet energy splitting ΔE_{st} of this N-heterocyclic carbene analogue, which will facilitate its chemical reactions. The theoretical findings originating from this study allow many predictions in experiments to be made.

Received 7th April 2021
Accepted 28th May 2021

DOI: 10.1039/d1ra02703d

rsc.li/rsc-advances

I. Introduction

The simple carbene (CH_2) is well known to be an electron-deficient two-coordinate carbon molecule, possessing two non-bonding electrons on the central carbon atom.[1] For over one hundred years, CH_2 and the carbene derivatives were always classified as only transient species since they were notoriously difficult to be experimentally isolated, let alone structurally characterized. Since 1991, the synthesis and isolation of thermally stable N-heterocyclic carbenes (NHCs) by Arduengo and co-workers[2] have greatly opened considerable research activity into the various fields of organic, inorganic, and organometallic chemistry.[3–21] For instance, many researches demonstrated that NHCs exhibit high tendency to act as strong σ-donors with a weak π-backbonding ability.[22] In particular, these NHC analogues exhibit the attractive natures with lower toxicity as well as higher air and thermal stability. As a result, NHCs are creating tremendous interests either in their ability of acting as versatile nucleophilic catalysts in a variety of organic designs[23–32] or as key ligands in many organometallic complexes, which mainly turned out to be useful components for broad applications.[33–40]

Through many sophisticated efforts by excellent synthetic chemists, the chemistry of monomeric four-, five-, and six-membered heterocycles of the general form **I–III** containing a pivotal group 13 element G13 (= B, Al, Ga, In, and Tl; Scheme 1) has been extensively studied in experiments in recent decades and still continues to be an active research area in many laboratories.[8–15] In this work, we devote our attention to the reactivity of the neutral six-membered NHC analogues featuring a group 13 element (**G13-6-Rea**). Although the understanding of the six-membered-ring **G13-6-Rea** molecules has certainly grown in recent years,[41–60] our knowledge concerning their relative chemical reactivity remains primitive compared to that of five-membered-ring NHC analogues

[a]*Department of Applied Chemistry, National Chiayi University, Chiayi 60004, Taiwan. E-mail: midesu@mail.ncyu.edu.tw*

[b]*Department of Medicinal and Applied Chemistry, Kaohsiung Medical University, Kaohsiung 80708, Taiwan*

† Electronic supplementary information (ESI) available. See DOI: 10.1039/d1ra02703d

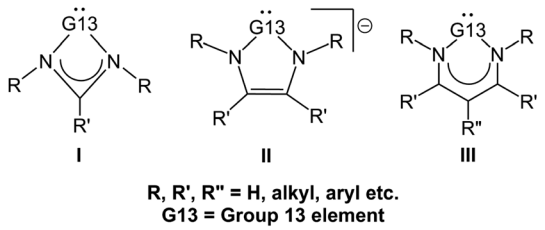

Scheme 1 General structures of group 13 element (G13) N-heterocycles.

bearing a central group 14 element.[22–25] In this study, we thus chose two typical chemical reactions (insertion, eqn (1), and cycloaddition, eqn (2)) based on density functional theory (DFT) to investigate the origin of the activation barriers for group 13 analogs of the six-membered NHCs.

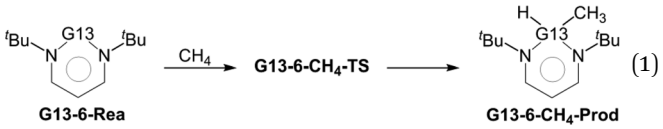

(1)

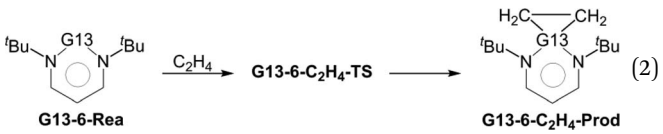

(2)

To gain better understanding of the chemical reactivity of **G13-6-Rea**, their chemical natures are analyzed in this work using three important fundamental concepts: aromaticity, basicity, and electrophilicity. Moreover, the sources of their activation barriers are studied with the VBSCD model[61–63] and the activation strain model (ASM)[64–67] method. Hopefully, our theoretical study focusing on the above fundamental concepts and electronic factors that characterize this six-membered-ring G13 family of NHC analogues will provide essential and useful information for understanding and explaining its chemical reactivity.

II. Methodology

A comprehensive computational gas-phase DFT study was performed using the Gaussian 09 E.0 software package[68] to optimize all molecular structures. Geometry optimizations were performed using the BP86 functional[69,70] including D3 dispersion corrections.[71,72] All atoms in this study were described with a def2-TZVP triple-ζ quality basis set.[73] We thus refer to the theoretical level as BP86-D3(BJ)/def2-TZVP. Frequency calculations at BP86-D3(BJ)/def2-TZVP were performed to identify either minimum energy geometries (zero imaginary frequencies) or transition states (one imaginary frequency). The pathway involving the initial reactants, transition states, and final products was examined by calculating the intrinsic coordinate (IRC).[74–76] Nucleus-independent chemical shift (NICS)[77–79] and anisotropy of the current-induced density (ACID)[80,81] calculations were performed using the GIAO method at BP86-D3(BJ)/def2-TZVP.

III. Results and discussion

(1) The geometries and electronic structures of G13-6-Rea (G13 = group 13 elements)

As mentioned in the Introduction, DFT was first used to study the model reactants **G13-6-Rea** (G13 = B, Al, Ga, In, and Tl), which feature *tert*-butyl substituents attached on the nitrogen atoms, by determining their geometrical and electronic structures. Our calculated BP86-D3(BJ)/def2-TZVP results for the key geometrical parameters and some physical properties of **G13-6-Rea** are shown in Table 1 (also see Fig. S1†).

To the best of our knowledge, no well-separated six-membered NHC monomer containing a pivotal boron element has been experimentally reported yet. Nevertheless, the experimental data concerning the G13–N bond distances in the six-membered NHCs with various substituents were reported as follows: Al–N (1.957 and 1.963 Å),[40,41] Ga–N (2.034–2.063 Å),[42,43]

Table 1 Key geometrical parameters for **G13-6-Rea** (G13 = group 13 elements) calculated at the BP86-D3(BJ)[a]/def2-TZVP[b] level of theory

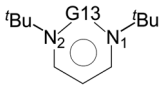

	B-6-Rea	Al-6-Rea	Ga-6-Rea	In-6-Rea	Tl-6-Rea
G13–N1 (Å)	1.429	2.045	2.143	2.377	2.480
G13–N2 (Å)	1.429	2.045	2.143	2.377	2.480
∠N1–G13–N2 (°)	121.4	92.28	88.42	85.78	78.92
ΔE_{st}[c] (kcal mol−1)	4.2	27.2	46.3	50.8	51.8
NICS(0)[d] (ppm)	−8.540	−1.476	−1.365	−1.185	−1.135
NICS(1)[e] (ppm)	−7.094	−3.250	−3.219	−2.367	−2.162
$NICS(1)_{zz}$[f] (ppm)	−7.002	−4.004	−3.841	−3.713	−2.735
PA[g] (kcal mol^{-1})	308.6	268.0	248.5	229.0	206.7
GPB[h] (kcal mol^{-1})	291.8	255.2	235.3	216.6	194.7
f_k^{+i}	−0.235	−0.141	−0.120	−0.266	−0.888
f_k^{-j}	−0.329	−0.703	−0.489	0.065	−0.147
μ^k (eV)	1.356	1.481	2.532	2.884	3.002
η^l (eV)	2.775	2.940	3.190	3.073	3.230
ω^m (eV)	2.551	3.224	10.23	12.78	14.54

[a] See ref. 69–72. [b] See ref. 73. [c] Energy relative to the corresponding singlet state. A positive value means that the singlet is the ground state. [d] NICS(0) stands for the NICS value calculated at the center of the molecular plane. [e] NICS(1) stands for the NICS value calculated 1.0 Å above the center of the molecular plane. [f] $NICS(1)_{zz}$ stands for the NICS value calculated at the zz component of the magnetic tensor NICS(1). [g] The proton affinity (PA) of **G13-6-Rea**, which is the reaction enthalpy based on the equation: (**G13-6-Rea**)$H^+_{(g)}$ → **G13-6-Rea**$_{(g)}$ + H^+. [h] The gas-phase basicity (GPB) of **G13-6-Rea**, which is the Gibbs free energy based on the equation: (**G13-6-Rea**)$H^+_{(g)}$ → **G13-6-Rea**$_{(g)}$ + H^+. [i] μ stands for the electronic chemical potential. For details see the text and Table S2. [j] η stands for the chemical hardness. For details see the text and Table S1. [k] ω stands for the electrophilicity index. For details see the text and Table S1. [l] f_k^+ stands for the nucleophilic attack. For details see Table S2. [m] f_k^- stands for the electrophilic attack. For details see Table S2.

In–N (2.268–2.364 Å),[44,45] and Tl–N (2.401–2.471 Å).[46,47] The corresponding BP86-D3(BJ)/TZVP data of **G13-6-Rea** provided in Table 1 agree reasonably well with the available experimental values.[40–47] Additionally, the experimental data for the central ∠N–G13–N bond angle were reported as follows: ∠N–Al–N (89.86° and 91.85°),[40,41] ∠N–Ga–N (87.53°–89.42°),[42,43] ∠N–In–N (78.23°–81.12°),[44,45] and ∠N–Tl–N (76.20°–78.00°).[46,47] Again, these attainable experimental values are in reasonably quantitative agreement with our BP86-D3(BJ)/TZVP results for the **G13-6-Rea** molecules. It must be noted that the computational and experimental results demonstrate that the central ∠N–G13–N bond angle in **G13-6-Rea** becomes more acute proceeding down the group 13 family from boron to thallium. This phenomenon can be attributed to the "inert s-pair effect" and "orbital non-hybridization effect," as discussed elsewhere.[82–85]

The singlet–triplet splitting ΔE_{st} ($= E_{triplet} - E_{singlet}$; kcal mol^{-1})[86] of **G13-6-Rea** (Table 1) follows the order **B-6-Rea** (3.9) < **Al-6-Rea** (28.2) < **Ga-6-Rea** (47.0) < **In-6-Rea** (51.0) < **Tl-6-Rea** (53.1). That is, ΔE_{st} increases monotonically from **B-6-Rea** to **Tl-6-Rea**. Fig. 1 shows that proceeding from **B-6-Rea** to **Tl-6-Rea**, a change of the group 13 element (G13) in **G13-6-Rea** decreases the energy of the nonbonded p^2-σ lone pair orbital, which is located at the pivotal G13 atom. Similarly, this G13 replacement down the group 13 family decreases the energy of the vertical p-π orbital at the G13 element. Furthermore, the theoretical data shown in Table 1 anticipates the small ΔE_{st} of **B-6-Rea** (4.2 kcal mol^{-1}), implying that this molecule could be kinetically unstable and readily undergo chemical reactions with other substrates. In fact, the previous studies have provided similarly small values of ΔE_{st} for borylenes.[87] The above theoretical finding could explain why the six-membered-ring boron NHC analogue has not been synthesized and stabilized in experiments.

However, it is noted that the BP86 method cannot provide correct orbital energies due to the reason that the BP86 method is composed of semi-local exchange, and, therefore, decays too rapidly instead of the correct $-1.00/R$ dependence. It has been shown that semi-local functional will collapse to the wrong HOMO–LUMO gap due to an incorrect description of the excitation binding energy in organic systems. For this reason, one single benchmark calculation using a range-separated functional such as LC-BLYP[88,89] has been utilized to draw the frontier molecular orbitals of **G13-6-Rea**, which is given in Fig. S2.† Fortunately, the energy order of the frontier molecular orbitals in Fig. S2† is quite similar to that in Fig. 1. We thus feel confidence for further studies about some properties of **G13-6-Rea** using the BP86 approach. For more details, one may find some useful references in the literatures.[90–92]

It is worth noting that the six-membered **G13-6-Rea** molecules studied in this work, the G13 atom and the molecular backbone (N–C–C–C–N) form an essentially planar six-membered ring. As a result, six π electrons are located in this

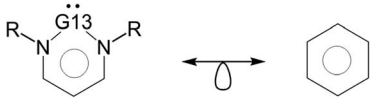

Scheme 2 **G13-6-Rea** is isolobal to benzene.

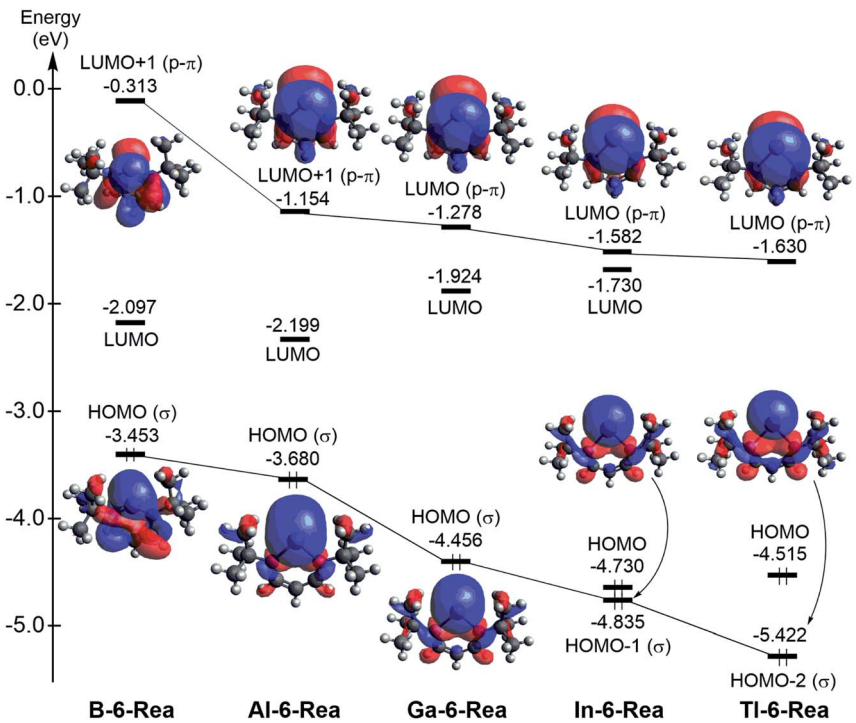

Fig. 1 Calculated frontier molecular orbitals of the **G13-6-Rea** (G13 = B, Al, Ga, In, and Tl) molecules at the BP86-D3(BJ)/def2-TZVP level of theory. For more information see the text.

molecular ring, implying that these cyclic **G13-6-Rea** molecules should have aromatic character. In fact, from the isolobal analogy viewpoint,[93] the six-membered-ring **G13-6-Rea** species is isolobal with benzene (C_6H_6), which owns the well-known high aromaticity (Scheme 2). Over the years, the nucleus-independent chemical shift (NICS) approach, developed by Schleyer and *et al.*,[77–79] has become one of the most popular aromaticity probes. We have thus applied the NICS index to investigate the aromatic nature of **G13-6-Rea**, whose computational NICS(0), NICS(1), and $NICS(1)_{zz}$ values are collected in Table 1. Table 1 shows that the NICS value of **G13-6-Rea** becomes smaller and less negative as its central G13 atom becomes heavier. These results can be ascribed to the nature of the pivotal G13 elements. In fact, both the orbital size and the orbital energy level of the valence np orbitals of the G13 atom play decisive roles in determining the aromatic character of **G13-6-Rea**. For instance, the six-membered ring skeleton of **B-6-Rea** contains only second row elements (B—N—C—C—C—N) and their valence 2p orbitals are similar in size.[94] Moreover, these valence 2p orbitals on the cyclic atoms of **B-6-Rea** are all close in orbital energy. As a result, these phenomena can easily form the p-π resonance on the six-membered ring and make **B-6-Rea** to possess the highest degree of aromaticity in the **G13-6-Rea** family. However, the frontier np orbitals of the heavy group 13 elements (such as Al, Ga, In and Tl) bear the higher principal quantum number n ($\geq$3), suggesting that both sizes and energy levels of the frontier np orbitals of a heavy G13 atom are quite larger than those of the valence 2p orbitals of a second row element. Therefore, unlike the significant delocalization over the B—N—C—C—C—N ring of **B-6-Rea**, there is effectively less overlap of the valence p-π orbital on the heavy G13 center with the two proximal N p-π orbitals. Accordingly, our theoretical analysis demonstrates that the aromatic character of the six-membered ring of **G13-6-Rea** decreases down the group 13 family from **B-6-Rea** to **Tl-6-Rea** (also see their ACID plots in Fig. S3†).

We are interested in the basicity of **G13-6-Rea**,[95] from which one may understand the nature of its chemical bonding with other substrates. We thus used the chemical equation ((**G13-6-Rea**)$H^+_{(g)}$ → **G13-6-Rea**$_{(g)}$ + H^+) to evaluate the proton affinity (PA) and gas-phase basicity (GPB) of **G13-6-Rea**, whose BP86 results are provided in Table 1. PA and GPB show a monotonically decreasing trend from **B-6-Rea** to **Tl-6-Rea**. The explanation for this phenomenon can be obtained from Fig. 1, in which the HOMO (highest occupied molecular orbital) of **B-6-Rea**, **Al-6-Rea**, and **Ga-6-Rea** is the nonbonding lone pair sp^2-σ orbital, which is located on the pivotal boron, aluminum, and gallium center of the corresponding heterocycle plane, respectively. Consequently, this theoretical evidence strongly suggests that **B-6-Rea**, **Al-6-Rea**, and **Ga-6-Rea** will display significant Lewis base chemistry. However, Fig. 1 shows that for **In-6-Rea** and **Tl-6-Rea**, the G13 p-π orbital, which is orthogonal to the six-membered ring, is largely associated with the LUMO. Therefore, our theoretical evidence indicates that **In-6-Rea** and **Tl-6-Rea** will exhibit Lewis acid chemical behavior.

An intriguing question is what role does **G13-6-Rea** play when it reacts with other substrates, *i.e.*, is it a nucleophile or an electrophile? The answer was obtained by applying the Fukui function,[96] the central site reactivity index of DFT, to the central G13 element of **G13-6-Rea**. The BP86 results summarized in Table 1 show that the calculated value of the Fukui function of nucleophilic attack (f_k^+) is obvious larger than that of electrophilic attack (f_k^-) for **B-6-Rea**, **Al-6-Rea** and **Ga-6-Rea**. This theoretical information strongly suggests that the above three molecules are nucleophilic and thus prefer to undergo nucleophilic attack with other substrates. The supporting evidence comes from the valence orbitals of **B-6-Rea**, **Al-6-Rea** and **Ga-6-Rea**, which are schematically illustrated in Fig. 1. That is, the HOMO (the nonbonding lone pair sp^2-σ orbital) of **B-6-Rea**, **Al-6-Rea** and **Ga-6-Rea** would play a dominant role in their chemical reactions. However, Table 1 shows that the Fukui function values of electrophilic attack (f_k^-) for **In-6-Rea** and **Tl-6-Rea** are apparently larger than those of the corresponding nucleophilic attack (f_k^+), indicating that the LUMO (the unoccupied vertical p-π orbital) of **In-6-Rea** and **Tl-6-Rea** plays a vital role in their chemical reactions. As a result, our theoretical evidence suggests that the **In-6-Rea** and **Tl-6-Rea** molecules should behave as strong electrophiles.

We also investigated the electrophilicity[97] of **G13-6-Rea**. As suggested by Koopmans,[98] Parr and coworkers,[99] the electronic chemical potential (μ), chemical hardness (η), and electrophilicity index (ω), respectively, were defined as follows:

$$\mu = -\frac{E_{HOMO} + E_{LUMO}}{2} \quad (3)$$

$$\eta = E_{LUMO} - E_{HOMO} \quad (4)$$

$$\omega = -\frac{\mu^2}{2\eta} \quad (5)$$

In principle, as with the traditional carbene species, the nature of the chemical reactivity of the six-membered NHC analogues **G13-6-Rea** depends on two competing frontier orbitals, *i.e.*, the nonbonding lone pair sp^2-σ orbital and the unoccupied vertical p-π orbital.[1] The same situations also apply to the **G13-6-Rea** species. Consequently, if the sp^2-σ lone pair orbital prevails, then the **G13-6-Rea** molecule manifests the nucleophilicity itself. Conversely, if the empty p-π orbital predominates, then the **G13-6-Rea** compound presents the electrophilicity itself. Table 1 clearly shows that the calculated values of the electrophilicity (ω) of **G13-6-Rea** increase in the order **B-6-Rea** (2.538) < **Al-6-Rea** (3.095) < **Ga-6-Rea** (1.180) ≪ **In-6-Rea** (11.78) < **Tl-6-Rea** (14.18). In other words, the larger the atomic number of the pivotal group 13 element in the six-membered ring is and the higher the electrophilicity of **G13-6-Rea** will be in chemical reactions. Again, the above theoretical observations can be verified from the frontier orbitals of **G13-6-Rea** depicted in Fig. 1. For instance, **B-6-Rea** has the sp^2-σ lone pair orbital as its HOMO, while its unoccupied vertical p-π orbital is much higher in energy than its LUMO. Therefore, this nonbonding lone pair sp^2-σ orbital (HOMO) plays an important role in governing the chemical reactivity of **B-6-Rea**. This result, in turn, makes **B-6-Rea** less electrophilic than the other **G13-6-**

Rea molecules. In contrast, **Tl-6-Rea** has the vertical p-π orbital on Tl as its LUMO, whereas its lone pair sp^2-σ orbital is much lower in energy than its HOMO. Consequently, one may easily foresee a crucial role for this empty vertical p-π orbital (LUMO) in the chemical behavior of **Tl-6-Rea**.[100]

Bearing the above theoretical findings in mind, we will use the concepts of aromaticity, basicity, and electrophilicity to explore the origin of barrier heights and the chemical reactivity of the **G13-6-Rea** molecules in the next section.

(2) The insertion reaction of G13-6-Rea (G13 = group 13 elements) with methane

We firstly examine the C–H bond insertion reaction of **G13-6-Rea** with methane (eqn (1)), whose calculated BP86-D3(BJ)/def2-TZVP results are schematically shown in Fig. 2. The computational Gibbs free activation energy ($\Delta G_{ACT,CH4}$) of the present study indicates that the larger the atomic number of the pivotal G13 atom is, the higher the activation energy of **G13-6-Rea** with methane will be, and its C–H bond insertion reaction will proceed with greater difficulty. For instance, the BP86 $\Delta G_{ACT,CH4}$ data (kcal mol^{-1}) given in Fig. 2 show that **B-6-CH$_4$-TS** (31.9) < **Al-6-CH$_4$-TS** (48.7) < **Ga-6-CH$_4$-TS** (64.1) < **In-6-CH$_4$-TS** (80.4) < **Tl-6-CH$_4$-TS** (100.4). This theoretical evidence strongly suggests that the C–H bond activation reactions of the six-membered group 13 NHC analogues with methane are kinetically unfavorable. The supporting evidences come from the experimental facts[55–59] that the six-membered ring Al analogue only breaks the C–C bond rather than the C–H bond of the hydrocarbons. Moreover, we investigated the theoretical results of their final insertion products (**G13-6-CH$_4$-Prod**). Again, from Fig. 2, the calculated Gibbs free energy of reaction ($\Delta G_{REA,CH4}$) follows the same trend as the atomic weight of the central G13 element, that is, **B-6-CH$_4$-Prod** (−32.2) < **Al-6-CH$_4$-Prod** (−17.9) < **Ga-6-CH$_4$-Prod** (5.6) < **In-6-CH$_4$-Prod** (27.8) < **Tl-6-CH$_4$-Prod**

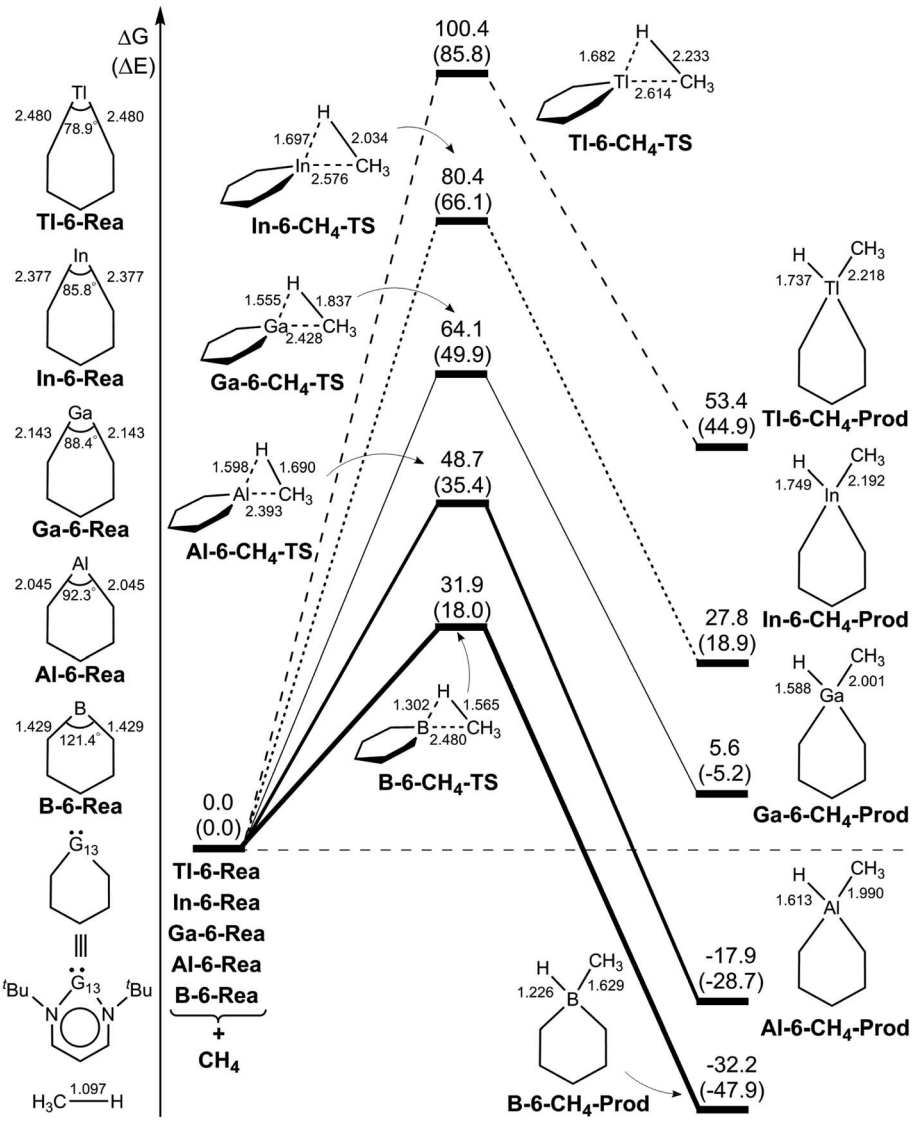

Fig. 2 BP86-D3(BJ)/def2-TZVP energy profiles (energy in kcal mol^{-1} and bond distances in Å) for the insertion reaction of **G13-6-Rea** (G13 = B, Al, Ga, In, and Tl) with CH_4. Also, see Fig. S4 and S5.†

Table 2 Energy decomposition analysis of methane activation by **G13-6-Rea** (G13 = group 13 elements) optimized at the BP86-D3(BJ)/def2-TZVP level of theory

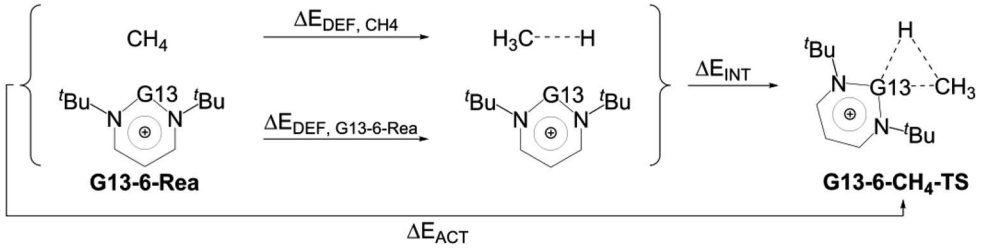

Entry	B-6-CH_4-TS	Al-6-CH_4-TS	Ga-6-CH_4-TS	In-6-CH_4-TS	Tl-6-CH_4-TS
$\Delta E_{ACT,CH4}$ [a,b]	18.8	35.4	49.9	66.1	85.8
$\Delta E_{DEF,CH4}$	38.6	58.0	71.4	87.8	101.8
$\Delta E_{DEF,G13\text{-}6\text{-}Rea}$	7.2	1.7	3.7	3.4	3.9
ΔE_{INT}	−27.8	−24.3	−25.2	−25.1	−19.9

[a] $\Delta E_{ACT,CH4} = \Delta E_{DEF,CH4} + \Delta E_{DEF,G13\text{-}6\text{-}Rea} + \Delta E_{INT}$. [b] All in kcal mol^{-1}.

(53.4). However, our above theoretical observations are based on the gas-phase calculations without involving the solvents. Additionally, the **B-6-Rea** molecule was theoretically proved to form thermodynamically stable product (Fig. 2). As a result, our present theoretical results cannot rule out C–H activation with the B analogue at high temperature in solution.

In addition, we found that using the valence bond state correlation diagram (VBSCD) model, which was originally developed by Shaik,[61–63] obtain a good linear relationship between the singlet–triplet energy splitting (ΔE_{st}) of **G13-6-Rea** and Gibbs free activation energy ($\Delta G_{ACT,CH4}$) as well as Gibbs free reaction enthalpy ($\Delta G_{REA,CH4}$) for its C–H bond insertion reaction with methane (Fig. 2). That is, $\Delta G_{ACT,CH4} = 1.17\Delta E_{st} + 22.4$ (the correction coefficient $r = 0.91$) (Fig. S6†) and $\Delta G_{REA,CH4} = 1.47\Delta E_{st} - 46.6$ ($r = 0.89$) (Fig. S7†). That is to say, the smaller the ΔE_{st} of **G13-6-Rea**, the lower the barrier height and, in turn, the faster the C–H bond activation reaction, and the greater the exothermicity. In other words, our theoretical results based on the VBSCD model demonstrate that ΔE_{st} can be a guideline for predicting the activation energy and reaction enthalpy of the C–H bond activation reaction of **G13-6-Rea** with hydrocarbons.

To gain a deeper understanding of the origin of the barrier heights for the C–H bond insertion reaction of **G13-6-Rea**, the activation strain model (ASM)[64–67] method was applied in this work. Table 2Table 3 shows that the activation energy ($\Delta E_{ACT,CH4}$) is separated into three terms, *i.e.*, the methane deformation energy ($\Delta E_{DEF,CH4}$), the **G13-6-Rea** deformation energy ($\Delta E_{DEF,G13\text{-}6\text{-}Rea}$), and the internal energy (ΔE_{INT}). Thus, they are schematically represented in Fig. 3 using the computational data collected in Table 2. Obviously, in the four curves,

Table 3 Energy decomposition analysis of ethene activation by **G13-6-Rea** (G13 = group 13 elements) optimized at the BP86-D3(BJ)/def2-TZVP level of theory

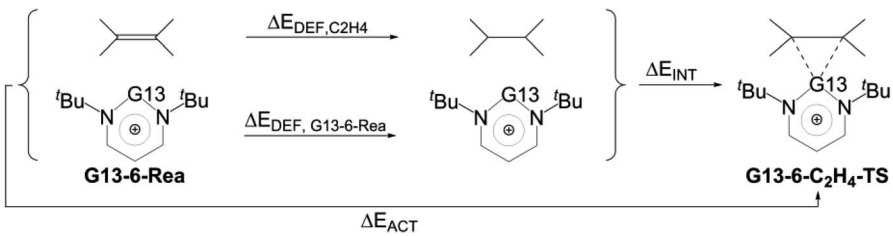

Entry	B-6-C_2H_4-TS	Al-6-C_2H_4-TS	Ga-6-C_2H_4-TS	In-6-C_2H_4-TS	Tl-6-C_2H_4-TS
$\Delta E_{ACT,C2H4}$ [a,b]	1.5	2.1	12.9	34.5	65.7
$\Delta E_{DEF,C2H4}$	7.2	13.2	22.3	38.5	53.6
$\Delta E_{DEF,G13\text{-}6\text{-}Rea}$	4.3	2.7	6.6	4.2	3.8
ΔE_{INT}	−10.0	−13.8	−16.0	−8.2	8.3

[a] $\Delta E_{ACT,C2H4} = \Delta E_{DEF,C2H4} + \Delta E_{DEF,G13\text{-}6\text{-}Rea} + \Delta E_{INT}$. [b] All in kcal mol^{-1}.

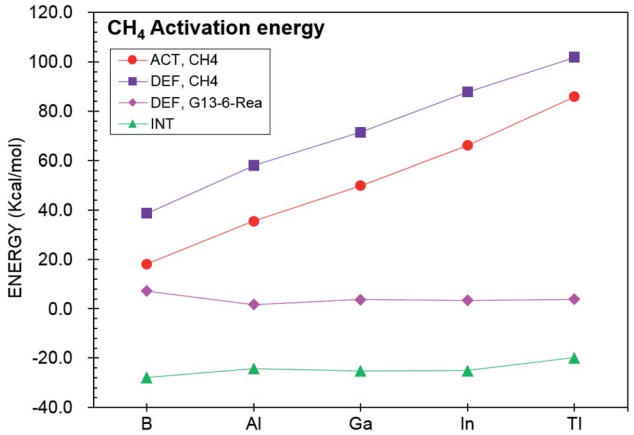

Fig. 3 Energy decompositions of the activation energies ($\Delta E_{ACT,CH4}$) of the transition states (**G13-6-CH$_4$-TS**) of the insertion reactions of **G13-6-Rea** (G13 = group 13 element) with CH_4. The data are taken from Table 2.

only $\Delta E_{DEF,CH4}$ increases monotonically down the group 13 family from **B-6-CH$_4$-TS** to **Tl-6-CH$_4$-TS**, following a trend identical to that of $\Delta E_{ACT,CH4}$. This result strongly suggests that the $\Delta E_{DEF,CH4}$ term is the dominant factor in determining the trend in the activation energy ($\Delta E_{ACT,CH4}$). Examining the BP86 geometrical structures of **G13-6-CH$_4$-TS** in Fig. 2 shows that the H…C stretching bond length (Å) in **G13-6-CH$_4$-TS** increases in the order 1.565 (**B-6-CH$_4$-TS**) < 1.690 (**Al-6-CH$_4$-TS**) < 1.837 (**Ga-6-CH$_4$-TS**) < 2.034 (**In-6-CH$_4$-TS**) < 2.233 (**Tl-6-CH$_4$-TS**). Note that the original H–CH_3 bond distance of methane was calculated to be 1.097 Å at the same level of theory. These calculated data can be explained as follows. In the transition state (**G13-6-CH$_4$-TS**), the H–CH_3 bond is breaking and the pivotal G13 element of **G13-6-Rea** is forming new bonds with the hydrogen and carbon atoms of methane. As a result, the increased elongation of the C–H bond length in the transition state for C–H activation moving down the G13 series is simply due to the Hammond postulate.[101] That is to say, as the **G13-6-CH$_4$-Prod** becomes higher in energy moving down G13, **G13-6-CH$_4$-TS** will more

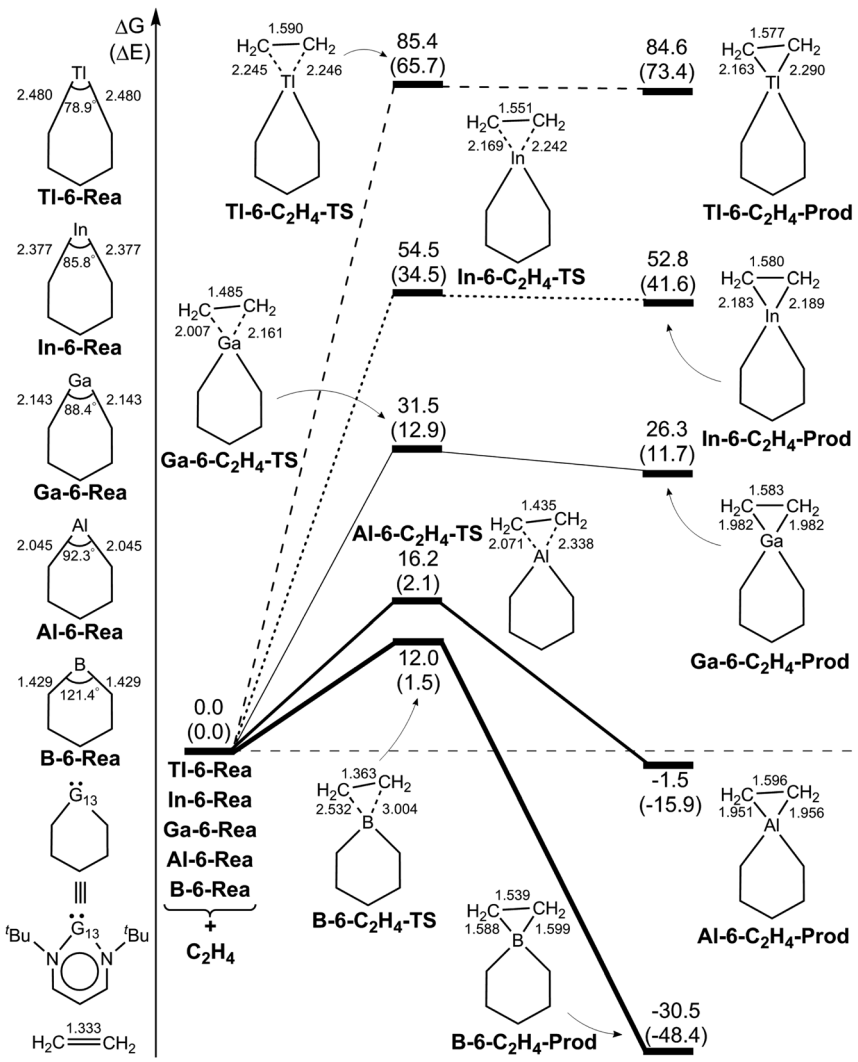

Fig. 4 BP86-D3(BJ)/def2-TZVP energy profiles (energy in kcal mol^{-1} and bond distances in Å) for the insertion reaction of **G13-6-Rea** (G13 = B, Al, Ga, In, and Tl) with $H_4C_2{=}C_2H_4$. Hydrogens are omitted in this picture for clarity. Also see Fig. S8 and S9.†

closely resemble products. This, in turn, makes the C–H bond length of methane in the **G13-6-CH_4-TS** will be longer as well as more product-like. Accordingly, our theoretical examination concludes that the trend in activation barriers of **G13-6-CH_4-TS** species is simply a consequence of both weaker G13–C and G13–H bonds in the product.

(3) The [1 + 2] cycloaddition reaction of G13-6-Rea (G13 = group 13 elements) with ethene

We next investigate the reactivity of **G13-6-Rea** toward the [1 + 2] cycloaddition to ethene (eqn (2)) at BP86-D3(BJ)/def2-TZVP. Fig. 4, which schematically represents the calculated results, demonstrates that the Gibbs free energy of activation ($\Delta G_{ACT,C2H4}$; kcal mol^{-1}) of **G13-6-C_2H_4-TS** increases monotonically down the group 13 family from boron to thallium. Specifically, **B-6-C_2H_4-TS** (12.0) < Al-**6-C_2H_4-TS** (16.2) < **Ga-6-C_2H_4-TS** (31.5) < **In-6-C_2H_4-TS** (54.5) < **B-6-C_2H_4-TS** (85.4). Moreover, the BP86 evidence in Fig. 4 indicates that the Gibbs free energy of reaction ($\Delta G_{REA,C2H4}$; kcal mol^{-1}) also increases in the order **B-6-C_2H_4-Prod** (−30.5) < Al-**6-C_2H_4-Prod** (−1.5) < **Ga-6-C_2H_4-Prod** (26.3) < **In-6-C_2H_4-Prod** (52.8) < **B-6-C_2H_4-Prod** (84.6). Notably, the relative energy of the cycloaddition product **B-6-C_2H_4-Prod** is below those of the corresponding reactants. However, the C–H activation reaction of **Al-6-Rea** with methane was theoretically predicted to be thermal-neutral. Our theoretical evidence therefore suggests that the [1 + 2] cycloaddition reaction between the six-membered-ring NHC analogue containing one central B element and ethene has favorable kinetics and thermodynamics.

On the basis of the VBSCD model[61–63] mentioned earlier, it was concluded that the **G13-6-Rea** molecule possessing a smaller value of ΔE_{st} ($= E_{triplet} - E_{singlet}$) should lead to a lower activation energy and a larger exothermicity. Indeed, the present computational results for the [1 + 2] cycloaddition reaction of **G13-6-Rea** with ethene confirm the accuracy of this prediction. Our BP86 data shown in Table 1 and Fig. 4 demonstrate a linear correlation between ΔE_{st} and the activation energy ($\Delta G_{ACT,C2H4}$, kcal mol^{-1}): $\Delta G_{ACT,C2H4} = 1.15\Delta E_{st} - 2.18$ ($r = 0.84$) (Fig. S10†). Likewise, a linear relationship is found between ΔE_{st} and the reaction free energy ($\Delta G_{REA,C2H4}$, kcal mol^{-1}): $\Delta G_{REA,C2H4} = 1.99\Delta E_{st} - 46.5$ ($r = 0.92$) (Fig. S11†). Accordingly, our theoretical findings suggest that the theoretical singlet–triplet energy splitting (ΔE_{st}) of the six-membered ring group 13 NHC analogue can be a measured criterion for predicting the reactivity.

Again, like the case of the C–H bond activation discussed earlier, the ASM[64–67] approach was used to explore the origin of the barrier heights of the cycloaddition reactions of **G13-6-Rea**. In Fig. 5, comparing the trend in the activation energy ($\Delta E_{ACT,C2H4}$) with those of its three components ($\Delta E_{DEF,C2H4}$, $\Delta E_{DEF,G13\text{-}6\text{-}Rea}$, and ΔE_{INT}), one finds that the ethene deformation energy ($\Delta E_{DEF,C2H4}$) is the key factor determining the trend in $\Delta E_{ACT,C2H4}$. This result can be explained in terms of the geometrical structures of **G13-6-C_2H_4-TS** given in Fig. 4. The BP86 data indicate that the stretching distance (Å) of the C…C bond in the ethene fragment of **G13-6-C_2H_4-TS** increases in the order 1.363 (**B-6-C_2H_4-TS**) < 1.435 (**Al-6-C_2H_4-TS**) < 1.485 (**Ga-6-C_2H_4-TS**) < 1.551 (**In-6-C_2H_4-TS**) < 1.590 (**Tl-6-C_2H_4-TS**). In comparison, the C=C double bond distance in the parent $H_2C{=}CH_2$ is 1.333 Å at the same level of theory. The above trend can be attributed to the atomic radius of the central G13 element in **G13-6-Rea**. During the attacking process between **G13-6-Rea** and ethene, both carbon atoms in the latter fragment must be separated for better orbital overlaps between the carbons and G13. As noted, the atomic radius of G13 increases with the atomic number.[102] As a result, the C–C bond distance of ethene in the transition state should increase with the atomic radius of G13. This phenomenon increases the bonding dissociation energy of ethene, which, in turn, increases the activation barrier, as demonstrated in Fig. 4. In brief, our theoretical observations indicate that the smaller the atomic radius of the pivotal group 13 element on the **G13-6-Rea** molecule is, the smaller ΔE_{st} of **G13-6-Rea**, the lower the activation barrier height, the faster the **G13-6-Rea** cycloaddition reaction with olefins, and the higher the reaction exothermicity of the cycloaddition product.

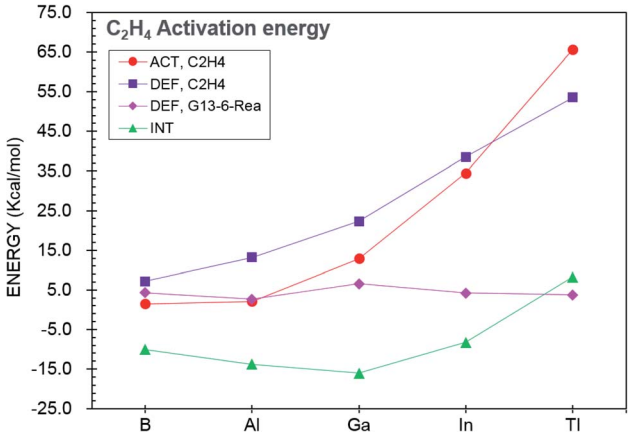

Fig. 5 Energy decompositions of the activation energies ($\Delta E_{ACT,C2H4}$) of the transition states (G13-6-C_2H_4-TS) of the [1 + 2] cycloaddition reactions of G13-6-Rea (G13 = group 13 element) with C_2H_4. The data are taken from Table 3.

IV. Conclusion

In this work, DFT accompanied by several well-established concepts (aromaticity/basicity/electrophilicity) and some sophisticated models (VBSCD[61–63] and ASM[64–67]) was used to explore the chemical reactivity of the six-membered-ring G13 NHC analogues (**G13-6-Rea**).

Interestingly, to date, no six-membered-ring boron NHC analogue has been prepared and synthesized in experiments. This can be explained in terms of the small ΔE_{st} of **B-6-Rea** (~4 kcal mol^{-1} according to our DFT data), which implies that this species is kinetically unstable and thus readily reacts with other substrates.

The present theoretical examinations show that the pivotal group 13 element in the six-membered ring of **G13-6-Rea** plays a crucial role in determining the chemical reactivity of this

molecule. Our theoretical analysis suggests that the HOMOs (the sp^2-σ lone pair orbital on the G13 element) are the key factors influencing the chemical behavior of **B-6-Rea**, **Al-6-Rea**, and **Ga-6-Rea**, and thus these molecules can be considered nucleophiles. In contrast, the LUMOs (the vacant p-π orbital on the G13 atom) are decisive factors controlling the chemical nature of **In-6-Rea** and **Tl-6-Rea**, and thus these molecules can be considered electrophiles. Moreover, the present study predicts that no **G13-6-Rea** molecule can undergo a C–H bond insertion reaction with hydrocarbons from kinetic and thermodynamic viewpoints. Indeed, recent experimental observations[55–59] indicate that the six-membered ring Al analogue only breaks the C–C bond rather than the C–H bond of the hydrocarbons. Nevertheless, our present theoretical observations cannot rule out **B-6-Rea** undergoing the C–H activation with hydrocarbons at high temperature in solution.

In addition, only **B-6-Rea** is a good candidate for [1 + 2] cycloaddition reactions with olefins. Furthermore, our theoretical predictions strongly suggest that the lower the atomic number of the group 13 element is, the smaller the atomic radius of the G13 atom, the higher the aromaticity of the six-membered ring of **G13-6-Rea**, and the smaller ΔE_{st} of this NHC analogue will be. This relationship, in turn, will pertain for all of its insertion reactions with hydrocarbons or cycloaddition reactions with olefins.

Conflicts of interest

There are no conflicts to declare.

Acknowledgements

The authors are grateful to the National Center for High-Performance Computing of Taiwan in providing huge computing resources to facilitate this research. They also thank the Ministry of Science and Technology of Taiwan for the financial support. Special thanks are also due to reviewers 1 and 2 for very helpful suggestions and comments.

References

1 W. Kirmse, in *Carbene Chemistry*, Academic Press, New York, 1st edn, 1964, ch. 1.
2 A. J. Arduengo III, R. L. Harlow and M. Kline, *J. Am. Chem. Soc.*, 1991, **113**, 361–363.
3 For annual reviews: *Coord. Chem. Rev.*, 2007, **251**, 595–895.
4 For annual reviews: *Chem. Rev.*, 2009, **109**, 3209–3884.
5 For annual reviews: *Eur. J. Inorg. Chem.*, 2009, 1663–2007.
6 For annual reviews: *Dalton Trans.*, 2009, 6873–7316.
7 D. Martin, M. Melaimi, M. Soleihavoup and G. Bertrand, *Organometallics*, 2011, **30**, 5304–5313.
8 See for example: M. Asay, C. Jones and M. Driess, *Chem. Rev.*, 2011, **111**, 354–396.
9 See for example: D. M. Flanigan, F. Romanov-Michailidis, N. A. White and T. Rovis, *Chem. Rev.*, 2015, **115**, 9307–9387.
10 See for example: R. Zhong, A. C. Lindhorst, F. J. Groche and F. E. Kühn, *Chem. Rev.*, 2017, **117**, 1970–2058.
11 See for example: H. V. Huynh, *Chem. Rev.*, 2018, **118**, 9457–9492.
12 See for example: V. Nesterov, D. Reiter, P. Bag, P. Frisch, R. Holzner, A. Porzelt and S. Inoue, *Chem. Rev.*, 2018, **118**, 9678–9842.
13 See for example: E. Peris, *Chem. Rev.*, 2018, **118**, 9988–10031.
14 See for example: A. Doddi, M. Peters and M. Tamm, *Chem. Rev.*, 2019, **119**, 6994–7112.
15 See for example: Á. Vivancos, C. Segarra and M. Albrech, *Chem. Rev.*, 2018, **118**, 9493–9586.
16 See for example: S. Kuwata and F. E. Hahn, *Chem. Rev.*, 2018, **118**, 9642–9677.
17 See for example: A. A. Danopoulos, T. Simler and P. Braunstein, *Chem. Rev.*, 2019, **119**, 3730–3961.
18 See for example: C. A. Smith, M. R. Narouz, P. A. Lummis, I. Singh, A. Nazemi, C.-H. Li and C. M. Crudden, *Chem. Rev.*, 2019, **119**, 4986–5056.
19 See for example: Q. Zhao, G. Meng, S. P. Nolan and M. Szostak, *Chem. Rev.*, 2020, **120**, 1981–2048.
20 See for example: Q. Zhao, G. Meng, S. P. Nolan and M. Szostak, *Chem. Rev.*, 2020, **120**, 1981–2048.
21 See for example: R. Jazzar, M. Soleilhavoup and G. Bertrand, *Chem. Rev.*, 2020, **120**, 4141–4168.
22 See for example: C. Boehme and G. Frenking, *J. Am. Chem. Soc.*, 1996, **118**, 2039–2046.
23 V. Nair, S. Bindu and V. Streekumar, *Angew. Chem., Int. Ed.*, 2004, **43**, 5130–5135.
24 D. Enders and T. Balensiefer, *Acc. Chem. Res.*, 2004, **37**, 534–541.
25 G. A. Grasa, R. M. Kissling and S. P. Nolan, *Org. Lett.*, 2002, **4**, 3583–3586.
26 G. A. Grasa, T. Guveli, R. Singh and S. P. Nolan, *J. Org. Chem.*, 2003, **68**, 2812–2819.
27 R. Singh, R. M. Kissling, M.-A. Letellier and S. P. Nolan, *J. Org. Chem.*, 2004, **69**, 209–212.
28 G. A. Grasa, R. S. Singh and P. Nolan, *Synthesis*, 2004, 971–985.
29 F. K. Zinn, M. S. Viciu and S. P. Nolan, *Annu. Rep. Prog. Chem., Sect. B: Org. Chem.*, 2004, **100**, 231–249.
30 R. Singh and S. P. Nolan, *Chem. Commun.*, 2005, 5456–5458.
31 T. Weskamp, W. C. Schattenmann, M. Spiegler and W. A. Herrmann, *Angew. Chem.*, 1998, **110**, 2631–2633.
32 T. Weskamp, W. C. Schattenmann, M. Spiegler and W. A. Herrmann, *Angew. Chem., Int. Ed.*, 1998, **37**, 2490–2493.
33 L. Ackermann, A. Furstner, T. Weskamp, F. J. Kohl and W. A. Herrmann, *Tetrahedron Lett.*, 1999, **40**, 4787–4790.
34 M. Scholl, T. M. Trnka, J. P. Morgan and R. H. Grubbs, *Tetrahedron Lett.*, 1999, **40**, 2247–2250.
35 J. Huang, H.-J. Schanz, E. D. Stevens and S. P. Nolan, *Organometallics*, 1999, **18**, 5375–5380.
36 W. A. Herrmann, *Synthetic Methods of Organometallic and Inorganic Chemistry*, Georg Thieme Verlag, Stuttgart, NY, 2000, vol. 9.
37 E. Peris and R. H. Crabtree, *Coord. Chem. Rev.*, 2004, **248**, 2239–2246.

38 C. M. Crudden and D. P. Allen, *Coord. Chem. Rev.*, 2004, **248**, 2247–2273.
39 N. M. Scott and S. P. Nolan, *Eur. J. Inorg. Chem.*, 2005, 1815–1828.
40 C. Cui, H. W. Roseky and H.-G. Schmidt, *Angew. Chem., Int. Ed.*, 2000, **39**, 4274–4276.
41 X. Li, X. Cheng, H. Song and C. Cui, *Organometallics*, 2007, **26**, 1039–1043.
42 N. J. Hardman, B. E. Eichler and P. P. Power, *Chem. Commun.*, 2000, 1991–1992.
43 D. Dange, S. L. Choong, C. Schenk, A. Stasch and C. Jones, *Dalton Trans.*, 2012, **41**, 9304–9315.
44 M. S. Hill and P. B. Hitchcock, *Chem. Commun.*, 2004, 1818–1819.
45 M. S. Hill, P. B. Hitchcock and R. Pongtavornpinyo, *Dalton Trans.*, 2005, 273–277.
46 Y. Cheng, P. B. Hitchcock, M. F. Lappert and M. Zhou, *Chem. Commun.*, 2005, 752–754.
47 C.-H. Chen, M.-L. Tsai and M.-D. Su, *Organometallics*, 2006, **25**, 2766–2773.
48 M. S. Hill, R. Pongtavornpinyo and P. B. Hitchcock, *Chem. Commun.*, 2006, 3720–3722.
49 H. Zhu, J. Chai, V. Chandrasekhar, H. W. Roesky, J. Magull, D. Vidovic, H.-G. Schmidt, M. Noltemeyer, P. P. Power and W. A. Merrill, *J. Am. Chem. Soc.*, 2004, **126**, 9472–9473.
50 T. Chu, S. F. Vyboishchikov, B. M. Gabidullin and G. I. Nikonov, *J. Am. Chem. Soc.*, 2017, **139**, 8804–8807.
51 C. Helling, C. Wölper and S. Schulz, *J. Am. Chem. Soc.*, 2018, **140**, 5053–5056.
52 R. Y. Kong and M. R. Crimmin, *J. Am. Chem. Soc.*, 2018, **140**, 13614–13617.
53 L. Song, J. Schoening, C. W. lper, S. Schulz and P. R. Schreiner, *Organometallics*, 2019, **38**, 1640–1647.
54 J. Krüger, C. Wölper, L. John, L. Song, P. R. Schreiner and S. Schulz, *Eur. J. Inorg. Chem.*, 2019, **11–12**, 1669–1678.
55 P. Bharadwaz and A. K. Phukan, *Inorg. Chem.*, 2019, **58**, 5428–5432.
56 C. Helling, C. Wölper, Y. Schulte, G. E. Cutsail III and S. Schulz, *Inorg. Chem.*, 2019, **58**, 10323–10332.
57 C. Helling, C. Wölper and S. Schulz, *Eur. J. Inorg. Chem.*, 2020, 4225–4235.
58 C. Bakewell, M. Garçon, R. Y. Kong, L. O'Hare, A. J. P. White and M. R. Crimmin, *Inorg. Chem.*, 2020, **59**, 4608–4616.
59 O. Kysliak, H. Görlsa and R. Kretschmer, *Dalton Trans.*, 2020, **49**, 6377–6383.
60 C. Helling, C. Wölper and S. Schulz, *Dalton Trans.*, 2020, **49**, 11835–11842.
61 S. Shaik, *J. Am. Chem. Soc.*, 1981, **103**, 3692–3701.
62 A. Pross, in *Theoretical and Physical principles of Organic Reactivity*, John Wiley & Sons Inc., USA, 1995.
63 S. Shaik and A. Shurki, *Angew. Chem., Int. Ed.*, 1999, **38**, 586–625.
64 T. Ziegler and A. Rauk, *Theor. Chim. Acta*, 1977, **46**, 1–10.
65 W.-J. van Zeist and F. M. Bickelhaupt, *Org. Biomol. Chem.*, 2010, **8**, 3118–3127.
66 F. M. Bickelhaupt and K. N. Houk, *Angew. Chem., Int. Ed.*, 2017, **56**, 10070–10086.
67 I. Fernándeza and F. M. Bickelhaupt, *Chem. Soc. Rev.*, 2014, **43**, 4953–4967.
68 M. J. Frisch, G. W. Trucks, H. B. Schlegel, G. E. Scuseria, M. A. Robb, J. R. Cheeseman, G. Scalmani, V. Barone, B. Mennucci, G. A. Petersson, H. Nakatsuji, M. Caricato, X. Li, H. P. Hratchian, A. F. Izmaylov, J. Bloino, G. Zheng, J. L. Sonnenberg, M. Hada, M. Ehara, K. Toyota, R. Fukuda, J. Hasegawa, M. Ishida, T. Nakajima, Y. Honda, O. Kitao, H. Nakai, T. Vreven, J. A. Montgomery, J. E. Peralta, F. Ogliaro, M. Bearpark, J. J. Heyd, E. Brothers, K. N. Kudin, V. N. Staroverov, R. Kobayashi, J. Normand, K. Raghavachari, A. Rendell, J. C. Burant, S. S. Iyengar, J. Tomasi, M. Cossi, N. Rega, J. M. Millam, M. Klene, J. E. Knox, J. B. Cross, V. Bakken, C. Adamo, J. Jaramillo, R. Gomperts, R. E. Stratmann, O. Yazyev, A. J. Austin, R. Cammi, C. Pomelli, J. W. Ochterski, R. L. Martin, K. Morokuma, V. G. Zakrzewski, G. A. Voth, P. Salvador, J. J. Dannenberg, S. Dapprich, A. D. Daniels, Ö. Farkas, J. B. Foresman, J. V. Ortiz, J. Cioslowski and D. J. Fox, *Gaussian 09, revision E.01*, Gaussian, Inc., Wallingford, CT, 2013.
69 A. D. Becke, *Phys. Rev. A*, 1988, **38**, 3098–3100.
70 J. P. Perdew, *Phys. Rev. B*, 1986, **33**, 8822–8824.
71 S. Grimme, S. Ehrlich and L. Goerigk, *J. Comput. Chem.*, 2011, **32**, 1456–1465.
72 S. Grimme, J. Antony, S. Ehrlich and H. Krieg, *J. Chem. Phys.*, 2010, **132**, 154104–154122.
73 F. Weigenda and R. Ahlrichsb, *Phys. Chem. Chem. Phys.*, 2005, **7**, 3297–3305.
74 K. Fukui, *J. Phys. Chem.*, 1970, **74**, 4161–4163.
75 K. Fukui, *Acc. Chem. Res.*, 1981, **14**, 363–368.
76 C. Gonzalez and H. B. Schlegel, *J. Chem. Phys.*, 1989, **90**, 2154–2161.
77 P. v. R. Schleyer, C. Maerker, A. Dransfeld, H. Jiao and N. J. v. E. Hommes, *J. Am. Chem. Soc.*, 1996, **118**, 6317–6318.
78 Z. Chen, C. S. Wannere, C. Corminboeuf, R. Puchta and P. v. R. Schleyer, *Chem. Rev.*, 2005, **105**, 3842–3888.
79 B. T. Psciuk, R. L. Lord, C. H. Winter and H. B. Schlegel, *J. Chem. Theory Comput.*, 2012, **8**, 4950–4959.
80 R. Herges and D. Geuenich, *J. Phys. Chem. A*, 2001, **105**, 3214–3220.
81 D. Geuenich, K. Hess, F. Kohler and R. Herges, *Chem. Rev.*, 2005, **105**, 3758–3772.
82 P. Pyykkö and J.-P. Desclaux, *Acc. Chem. Res.*, 1979, **12**, 276–281.
83 W. Kutzelnigg, *Angew. Chem., Int. Ed. Engl.*, 1984, **23**, 272–295.
84 P. Pyykkö, *Chem. Rev.*, 1988, **88**, 563–594.
85 P. Pyykkö, *Chem. Rev.*, 1997, **97**, 597–636.
86 In this work, the unpaired spins in the triplet configuration reside on the HOMO and the LUMO of the **G13-6-Rea** species rather than the sp^2-σ lone pair orbital and the vacant p-π orbital on the pivotal group 13 element.
87 Y. Wang and C.-G. Liu, *Phys. Chem. Chem. Phys.*, 2020, **22**, 28423–28433.

88 O. A. Vydrov and G. E. Scuseria, *J. Chem. Phys.*, 2006, **125**, 234109–234117.
89 O. A. Vydrov, J. Heyd, A. Krukau and G. E. Scuseria, *J. Chem. Phys.*, 2006, **125**, 074106–074114.
90 M. Hagemann, R. J. F. Berger, S. A. Hayes, H.-G. Stammler and N. W. Mitzel, *Chem.–Eur. J.*, 2008, **14**, 11027–11038.
91 K. R. Leopold, M. Canagaratna and J. A. Phillips, *Acc. Chem. Res.*, 1997, **30**, 57–64.
92 J. J. C. Trujillo and I. Fernández, *Chem.–Eur. J.*, 2018, **24**, 17823–17831.
93 R. Hoffmann, *Angew. Chem., Int. Ed.*, 1982, **21**, 711–724.
94 A. Liberles, *J. Chem. Educ.*, 1977, **54**, 479–482.
95 L. D. Betowski, J. J. Solomon and R. F. Porter, *Inorg. Chem.*, 1972, **11**, 424–427.
96 P. W. Ayers and R. G. Parr, *J. Am. Chem. Soc.*, 2000, **122**, 2010–2018.
97 P. K. Chattaraj, U. Sarkar and D. R. Roy, *Chem. Rev.*, 2006, **106**, 2065–2091.
98 T. A. Koopmans, *Physica*, 1933, **1**, 104–113.
99 R. G. Parr, L. v. Szentpály and S. Liu, *J. Am. Chem. Soc.*, 1999, **121**, 1922–1924.
100 In this work, we have discussed whether the **G13-6-Rea** molecules would behave as electrophiles or nucleophiles in interactions with a substrate. For instance, we have utilized the concepts of Fukui functions to anticipate that **B-6-Rea**, **Al-6-Rea**, and **Ga-6-Rea** would react as nucleophiles, while **In-6-Rea** and **Tl-6-Rea** would act as electrophiles. Nevertheless, it is accepted that many real examples have shown that their chemical reactivity is not governed by the HOMO/LUMO of the reacting molecules. It could be the other adjoining frontier molecular orbitals (such as, HOMO−1 or LUMO−1) that can control the chemical reactivity due to their molecular orbital patterns, symmetries, and the relative energies compared with those of the reacting substrates. As a result, according to the frontier molecular orbitals shown in Fig. 1, it is likely all **G13-6-Rea** act as ambiphilicity. This, in turn, would make the reacting substrates interact with **G13-6-Rea**, which should be reexamined to determine the natures of these reactions. Such researches, however, are beyond the scope of the present work.
101 G. S. Hammond, *J. Am. Chem. Soc.*, 1955, **77**, 334–338.
102 B. Cordero, V. Gómez, A. E. Platero-Prats, M. Revés, J. Echeverría, E. Cremades, F. Barragán and S. Alvarez, *Dalton Trans.*, 2008, **37**, 2832–2838.